ACS OMEGA

Open Access

http://pubs.acs.org/journal/acsodf

Article

Advanced Equilibrium Studies for the Synergetic Impact of Polyaniline on the Adsorption of Rhodamine B Dye by Polyaniline/Coal Composite

Mohamed Adel Sayed, Abdelrahman Mohamed, Sayed A. Ahmed, Ahmed M. El-Sherbeeny, Wail Al Zoubi,* and Mostafa R. Abukhadra*

Cite This: *ACS Omega* 2023, 8, 47210−47223

Read Online

ACCESS | Metrics & More | Article Recommendations | Supporting Information

ABSTRACT: The synergetic improvement effect of the polyaniline (PANI) hybridization process on the adsorption of rhodamine B dye (RB) by PANI/coal hybrid material (PANI/C) has been evaluated using both traditional equilibrium modeling and advanced isotherm investigations. The composite was prepared by polymerizing polyaniline in the presence of coal fractions with a surface area of 27.7 m^2/g. The PANI/C hybrid has an improved capacity to adsorb RB dye (423.5 mg/g) in comparison to coal particles (254.3 mg/g). The maintained increase in the elimination properties of PANI/C has been illustrated using the steric characteristics of active site density (Nm) as well as the total number of adsorbed RB on a single active site (n). However, the incorporation of PANI did not yield any substantial impact on the existing active sites' quantity, but the hybridization processes greatly influenced the selectivity and affinity of each active site, in addition to the aggregation characteristics of the dye as it interacts with the composite's surface. Whereas raw coal can only adsorb three molecules of RB, each active site throughout the PANI/C surface can adsorb approximately eight RB molecules. This is also evidence of RB dye adsorption in a vertical arrangement, which involves multimolecular processes. The Gaussian energy (4.01−5.59 kJ/mol) and adsorption energy (−4.34−4.68 kJ/mol) revealed the controllable impact of physical mechanisms. These mechanisms may include van der Waals forces, dipole−dipole interactions, and hydrogen bonds (<30 kJ/mol). The thermodynamic functions, such as enthalpy, internal energy, and entropy, that have been assessed provide evidence supporting the exothermic and spontaneous nature of the RB uptake processes by PANI/C.

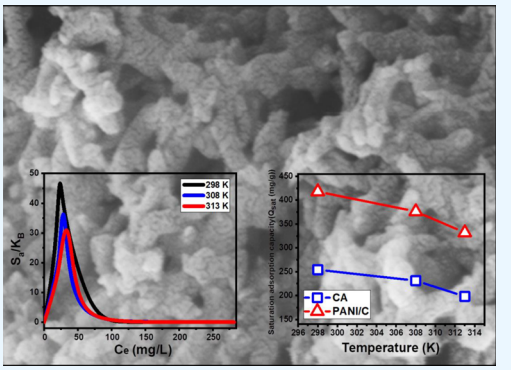

1. INTRODUCTION

The contamination of different water resources and clean water supplied with hazardous chemicals is the most important threat to the contemporary world and its residents' safety.[1,2] By 2025, 50% of the global population will face water shortages, according to a severe warning from the World Health Organization (WHO).[1,3] Accelerated growth in industries in recent decades has been reflected in substantial environmental challenges, such as contaminants in water and their detrimental effects on both humans and aquatic habitats.[1,2] Microbes, chemical pesticides, heavy metals, pharmaceutical residues, and dyes were among the common water contaminants discharged by industrial activities.[4,5] Synthetic dyes are a broad class of aromatic organic chemicals that are used as coloring agents in numerous types of industries, including paper, plastics, leather, the printing process, and clothing.[6,7] As a consequence, nearly 7×10^5 tons of the manufactured dyes have been estimated to be discharged into the environment as well as aquatic habitats each year.[8]

Most synthetic dyes are dangerous, nonbiodegradable substances with potential harmful impacts on human beings and the environment.[8,9] Among the synthetic dyes, rhodamine B (RB) was extensively used in the paper printing, leather dyeing, steel, textile, paint, and food industries.[10] It was classified as a carcinogenic cationic xanthine dye that has high solubility properties (15.0 g L^{-1} at 20 C).[11−13] The existence of RB dye in the water supplies and the aquatic environments displays strong toxicity (genotoxic and neurotoxic) on both humans and animals, in addition to several serious risks such as respiratory disorders, congestion of the skin, and gastro-intestinal injury.[10,13,14] As a result, the elimination of RB and other synthetic dyes from water using novel and low-cost operations was prioritized at later intervals.[13,14]

Received: September 23, 2023
Revised: October 27, 2023
Accepted: November 16, 2023
Published: December 1, 2023

Adsorption has been suggested as an effective technique for removing soluble dyes owing to its facile use, excellent effectiveness, recycling potential, large-scale practical application, and low cost of manufacturing.[13,15] As a result, natural accessibility, manufacturing cost, rapid kinetic rates, adsorption performance, adsorption specificity, and reusable functionality are the main characteristics for selecting the most effective adsorbents.[9] Consequently, it was strongly urged to establish innovative structures that have enhanced adsorption capacities by implementing naturally existing precursors that are low-cost and widely available to accomplish both environmental and economic objectives.[2] Moreover, heterogeneous and multifunction frameworks derived from naturally occurring precursors containing complex organic/inorganic reacting chemical groups have been evaluated as more favorable affordable adsorbents during the elimination of different species of organic compounds and molecules that exist as contaminants in the water supplied and the aquatic environments.[16,17]

Recent studies have demonstrated that natural coal, either in its unmodified or modified varieties, is a highly effective, inexpensive, easily accessible, and naturally adsorbent, exhibiting a great affinity for organic chemicals, including synthetic dyes.[17−19] It is composed of a series of aromatic polycyclic hydrocarbons that are linked chemically by a number of oxygen-rich reactive functional groups, including carbonyl, carboxyl, hydroxyl, and phenolic groups among them.[20,21] Such oxygen-rich functionalities possess significant reactivity to be successfully used as adsorbents or to be incorporated in composites including various inorganic and organic compounds.[19−21] Therefore, it was expected that the hybridization of coal with a polymer like polyaniline might yield an attractive hybrid material with enhanced properties as adsorbent.

Polyaniline has piqued the interest of researchers as an attractive conducting polymer with excellent surface area, substantial stability, high adsorption capacity, nontoxicity, affordable cost, and great environmental advantages.[22−24] The surface of the PANI has high adsorption affinities toward the soluble dye molecules, involving different mechanisms such as pi−pi interaction, electrostatic interaction, and H-bonding.[25,26] Additionally, the polymeric structure of PANI contains numerous amine and imine functional groups with a single pair of electrons that also induce its adsorption capacity.[25,27] Therefore, the coating of the PANI framework on the surfaces of the other materials in the literature resulted in extremely significant structures that exhibited excellent effectiveness in the reduction of common contaminants from wastewaters.[4,28,29] This includes its integration with magnetite, cuprous oxide, CNTs, graphite, fibers, graphene, and zeolite.[22−25] However, most of the structures are of no sufficient natural availability and still have high costs, low affinities for organic compounds, and complicated synthesis procedures as compared to structure of coal.

The integration between coal and polyaniline in composites can result in facilely fabricated and low-cost hybrids of significantly enhanced adsorption properties and decontamination efficacies for synthetic dyes to be applied in practical decolorization processes. As a result, the main objective of this study is to develop a polyaniline/coal blend (PANI/C) as a multifunctional adsorbent that possesses enhanced adsorption properties for the RB dye. This was accomplished by implementing the synergistic effects of polyaniline on the characteristics of coal based on all of the experimental factors and using theoretical modeling. The mathematical modeling included investigating both traditional and advanced models to predict the active site density, saturation capacity of adsorption, number of adsorbed ions, adsorption energy, and thermodynamic functions.

2. RESULTS AND DISCUSSION

2.1. Characterization of the Adsorbent. The XRD pattern of the synthesized PANI/C hybrid was compared to the diffraction characteristics of the basic components that were incorporated, including fresh coal as well as PANI (Figure 1). The diffraction peaks of natural coal demonstrate the

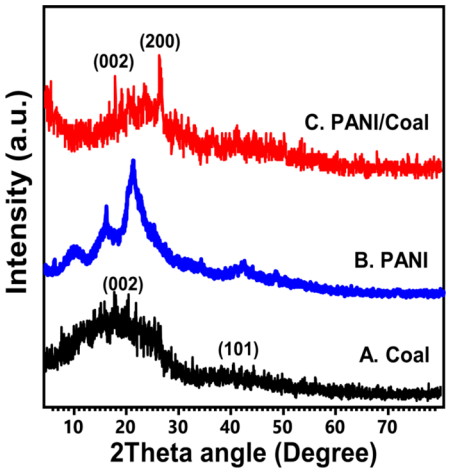

Figure 1. XRD patterns of raw coal (A), polyaniline (B), and synthetic PANI/C composite (C).

typical broad diffraction peaks (8−30° (002) and 40−50° (101)) of noncrystalline or amorphous carbon-derived or carbonaceous materials (Figure 1A).[17] The free form of the employed polyaniline (PA) displays a pattern of semicrystalline structures containing two peaks around 20 and 26° (Figure 1B). The observed peaks in the XRD pattern corresponding to the PANI/coal hybrid imply that coal and PANI chains were successfully integrated during its synthesis by instantaneous polymerization for aniline monomers in the presence of coal particles (Figure 1C). The pattern revealed the presence of an extra peak at 27.5° (200), which corresponds to the principal peak of PANI and reflects its semicrystalline characteristics [30].

The scanning electron microscopy (SEM) photos of the synthesized polyaniline/coal (PANI/C) composite reveal a noticeable presence of the PA polymer on the coal-layered particulates (Figure 2). The existence of the PANI was easily identified by its network of intersecting nanorods (Figure 2A). These intersected nanorods trigger the formation of a porous layer containing secondary nanopores and a rough topography on the coal, resulting in a noticeable rise in its surface area (Figure 2B,C). This was corroborated by the sample's HRTEM photographs, which showed that PANI-tabulated or rodlike nanoparticles exist as intersected nanoparticles developing network structures on the smooth outer layer of coal particles (Figure 2D). It is worth mentioning that the integration of PA and its interaction with the surface of coal resulted in noticeable changes in its network structures as well as the length, section, and shapes of its rods (Figure S1). The

https://doi.org/10.1021/acsomega.3c07355
ACS Omega 2023, 8, 47210−47223

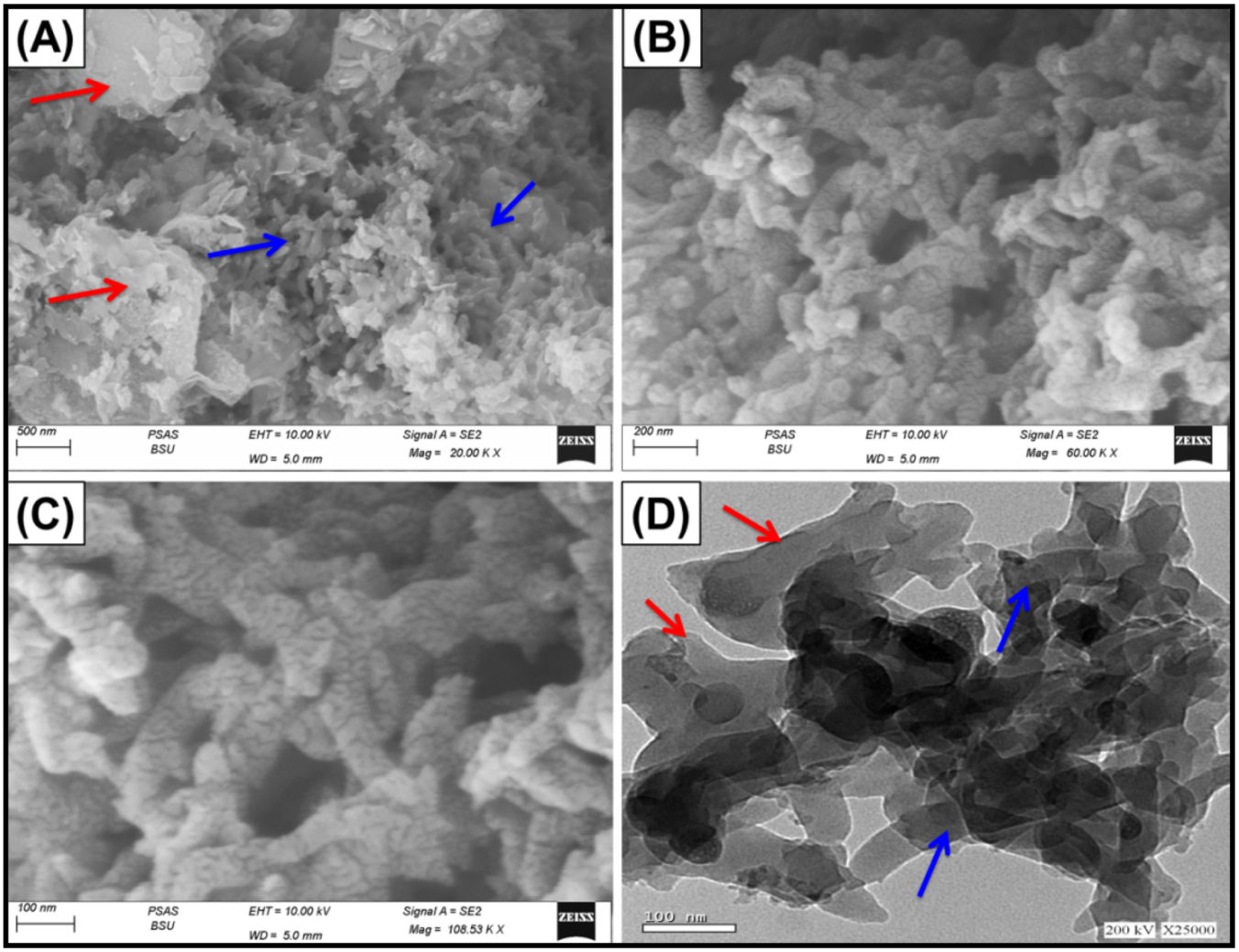

Figure 2. SEM images of the synthetic PANI/C composite (A), high-magnification SEM images for the polyaniline structure on the surface of coal (B, C), and HRTEM image of the synthetic PANI/C composite (D) (notice: red arrows refer to coal, and blue arrows refer to PANI).

morphological impact of the coated PANI layer significantly affected the textural properties of the PANI/C composite. The measured N_2 adsorption/desorption isotherm curve exhibits an IV type that has a prominent H3-type hysteresis loop. This verifies the nanoporous (mesoporous) features of PANI/C, which mainly correspond to the evacuating and/or filling of tabulated or cylinder-like nanopores through capillary condensation processes.[12,31] This assignment mostly pertains to the described morphologies of the intersecting PANI tabular grains in the network structure. The surface area of PANI/C was determined to be 27.7 m^2/g, which indicates a very favorable result for evaluating the product's potential as an adsorbent.

The alterations in the essential chemical groups were monitored by analyzing the FTIR spectra of the composite material and each of its components (Figure 3). The raw specimen exhibited the characterization of the basic chemical constituents that comprise natural coal (Figure 3A). The identified chemical groups include carboxylic and/or alcoholic O−H groups formed by hydrogen binding in coal (3000−3600 cm^{-1}). Additionally, COOH groups were observed at 1716 cm^{-1}, asymmetrical aliphatic C−H (SP3) at 2858 cm^{-1}, symmetrical aliphatic C−H (SP3) at 2940 cm^{-1}, aromatic C−C at 1616 cm^{-1}, C−H in functional methylene groups at 1450

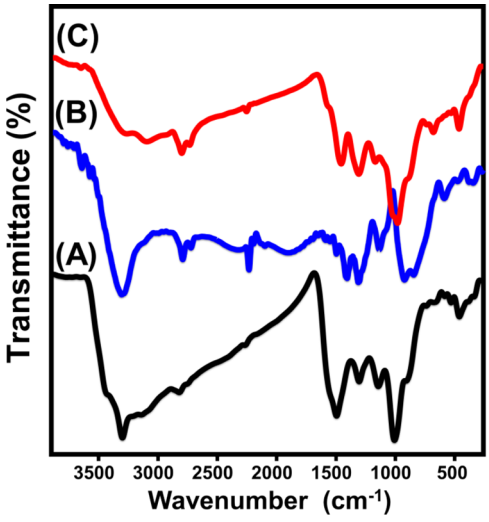

Figure 3. FTIR spectra of raw coal (A), polyaniline (B), and the synthetic PANI/C composite (C).

cm^{-1}, C−H in structural methyl groups at 1372 cm^{-1}, C−O within the range of 1000−1200 cm^{-1}, and aromatic C−H within the range of 500−900 cm^{-1} (Figure 3A).[17,32,33] The

https://doi.org/10.1021/acsomega.3c07355
ACS Omega 2023, 8, 47210−47223

infrared spectra of the synthesized PANI/C blend (Figure 3C) were evaluated and compared to the spectra of PANI (Figure 3B) and coal (Figure 3A). The PANI spectrum has distinct identifying bands corresponding to its polymeric chemical structure. The observed spectral bands correspond to specific functional groups of PANI: N−H (3401 cm^{-1}), aromatic C−H (2918 cm^{-1}), C−N (1105 cm^{-1}), C═C in quinoid rings (1467 cm^{-1}), C═C in benzenoid rings (1301 cm^{-1}), C−H (789 cm^{-1}), and C−H in the para-aromatic rings (587 cm^{-1}) (Figure 3B).[34,35]

The PANI/C spectrum exhibits intricate bands that arise from the interaction between the coal surface and the integrated PANI polymer (Figure 3C). The confirmation of the effective integration of PA was verified by detecting certain identifying bands from the spectra of PANI/C at deviated positions. The spectral analysis of PANI/C revealed distinct bands centered on 1590 and 1450 cm^{-1}, which were attributed to the bending deformation of C═C bonds in the structural quinoid as well as the benzenoid rings of PANI, respectively (Figure 3C).[30,36] The spectra of the composite material exhibited additional identifying bands of PANI at about 2350 cm^{-1} (corresponding to the C≡N bond) plus two additional bands at 1295 and 1130 cm^{-1} (associated with the C−N bond for secondary aromatic amine) (Figure 3C).[30,37] Moreover, a noteworthy combination exists between certain organic functional groups of PANI and coal. This is evident from the detectable bands of C−H vibrations that are approximately around 670 cm^{-1}, which exhibit a significant enhancement in their intensity. This enhancement indicates the successful coating of the coal surfaces with chains of PANI (Figure 3C).

2.2. Adsorption Results. *2.2.1. Effect of the pH.* The pH factor plays an essential role in an adsorption reaction as it influences both the adsorbent's surface charge and the ionization characteristics of soluble contaminants in water-based solutions. Along with a pH range of 3 to 10, additional variables were kept constant at 200 mL for the treated volume, 50 mg/L for the RB concentration, 120 min for contact time, 0.2 g/L for dosage, and 25 °C for the temperature of the experiment. These parameters have been employed to examine the adsorption behaviors of CA and PANI/C during the elimination of the RB dye. The experimental results indicate that the adsorption of RB utilizing both CA and PANI/C materials exhibited a noticeable enhancement when the pH of the contaminated solutions increased from pH 2 to pH 8 (Figure 4). At pH 8, the RB adsorption capacities improved from 15.6 mg/g (CA) and 20.7 mg/g (PANI/C) to 68.2 mg/g (CA) and 83.4 mg/g (PANI/C) (Figure 4). Afterward, a discernible decrease could be observed when the pH increased from pH 8 to 10, resulting in uptake values of 48.6 mg/g (CA) and 70.6 mg/g (PANI/C) (Figure 4). As a result, the assessed structures will possess the required characteristics to serve as remarkably effective adsorbents for realistic remediation activities that target RB dye, aligning with the pH range specified for industrial wastewater by the US EPA (pH 6 to 9).[38] The ionization behavior of RB, in addition to the dominant surficial charges of CA and PANI/C, may be used to illustrate the claimed variations in the uptake qualities.

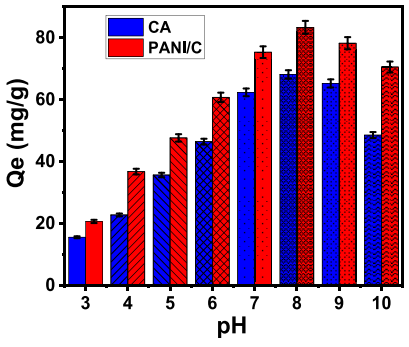

Figure 4. Influence of the solution pH on the uptake of RB by CA and PANI/C.

Based on the determined values of the isoelectric point or the point of zero charge ($pH_{(PZC)}$) of CA (7.8) and PANI/C (8.2), their surfaces are highly saturated with negative charges at pH levels higher than these values and positive charges at pH conditions lower than them.[39,40] The dominant positive charges at low-pH conditions are assigned to the protonation of the coal functional groups and the imine groups of PANI. Therefore, their surfaces have remarkable electrostatic repelling properties against the cationic RM molecules.[25,41] This is in agreement with the reported pK_a values of RB (3), i.e., the dye molecules have positive charges at pH less than 3.[41] Consequently, the increment in pH resulted in a declination in the density of the present positive groups and an increase in the quantities of the negatively charged groups, inducing the uptake performances of RB by both CA and PANI/C by the electrostatic attractions up to pH 8.[12,19] Beyond pH 8, the extensively negatively charged groups of CA and PANI/C display noticeable electrostatic repulsion with the RB molecules that exist in their zwitterionic form at these conditions, causing a drop in the uptake effectiveness.[25]

2.2.2. Kinetic Studies. 2.2.2.1. Effect of Contact Time. The significance of the adsorption duration on the established discoloration capacities of RB via CA and PANI/C has been studied in an experimental investigation. The adsorption duration was varied within a range of 30 to 840 min, maintaining the concentration of RB at 50 mg/L, the dosage at 0.2 g/L, the total volume at 200 mL, the temperature at 25 °C, and the pH at 8. The discoloration properties of coal (CA) and its composite material (PANI/C) as potential adsorbents for RB dye demonstrate significant enhancements in both adsorption rates and capacity (measured in mg/g) in terms of the controlled prolongation of the testing duration (Figure 5A). The noticeable improvement impacts were set at duration of 240 min for CA and 360 min for PANI/C. Subsequently, the extra duration of the tests demonstrates negligible impacts with regard to the rates of adsorption or the quantities of the sequestered RB. This indicates a state of stabilization or equilibrium conditions (Figure 5A). Under this condition, the RB dye adsorption capacities of CA and PANI/C particulates (111.3 mg/g for CA and 140.5 mg/g for PANI/C) are at equilibrium (Figure 5A). The significant increase in the adsorption of RB and its quick rates may be attributed to the high availability of empty active sites on the surfaces of CA and PANI/C particulates during the first stages of the discoloration processes.[3] As the duration of testing increases, there is a progressive rise in the adsorption of RB into CA and PANI/C empty sites. Consequently, these sites undergo occupation and depletion, leading to a significant reduction in their availability. Therefore, there was a notable drop in the actual rates of adsorption observed across a particular time interval, whereas the CA and PANI/C particulates displayed negligible enhancements in their adsorption properties. The equilibrium state of

https://doi.org/10.1021/acsomega.3c07355
ACS Omega 2023, 8, 47210−47223

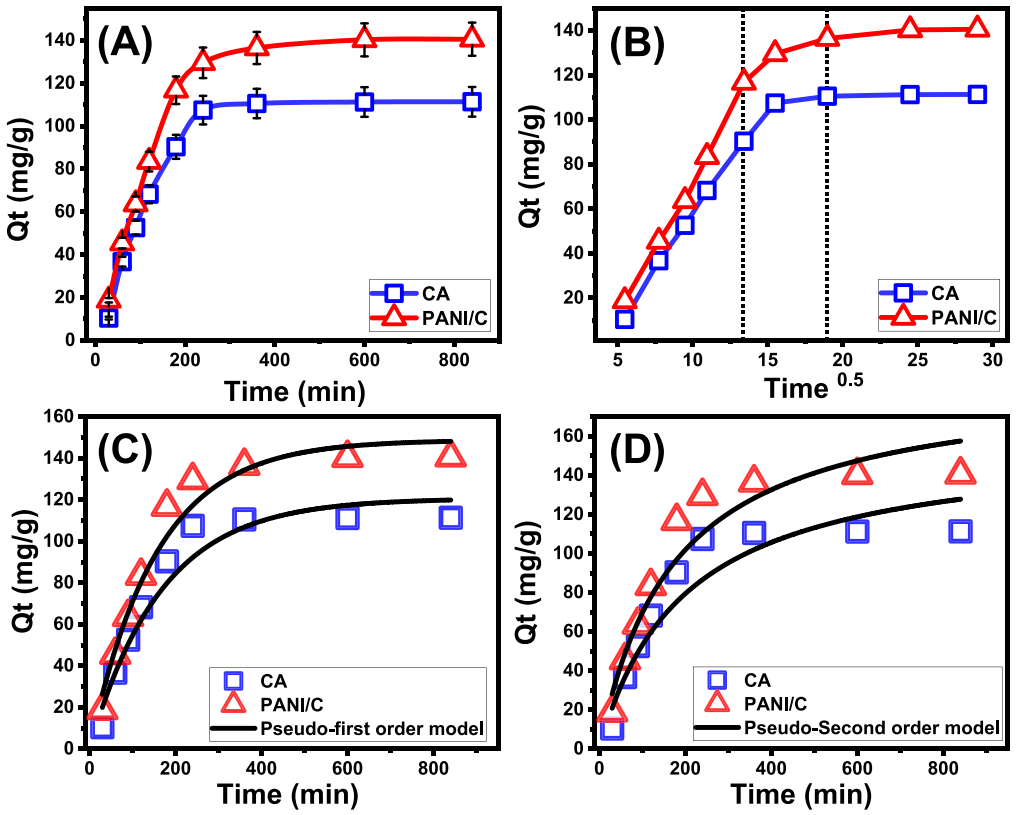

Figure 5. Influence of the contact time on the uptake of RB by CA and PANI/C (A), the intraparticle diffusion curves of the RB uptake reactions (B), fitting of the RB adsorption behaviors with the pseudo-first-order kinetic model (C), and fitting of the RB adsorption behaviors with the pseudo-second-order kinetic model (D).

CA and PANI/C has been determined after the saturation of all existing sites with RB molecules.[4]

2.2.2.2. Intraparticle Diffusion Behavior. RB adsorption systems accomplished using CA and PANI/C exhibit intraparticle diffusion curves that display segmentation features and demonstrate three different phases that do not intersect with the beginning points of the curves (Figure 5B). This finding indicates that the uptake of RB molecules involves collaborative mechanisms, besides the major influence of the diffusion of the dye ions in the direction of the active sites of CA and PANI/C.[42,43] The mechanisms may include (A) the adsorption of RB onto active sites that exist on the outer surface; (B) the diffusion of RB into the particulates; and (C) the influence of the saturation or equilibrium phases.[44] The first step shows that the RB's external adsorption pathways were active once the testing began and the efficacy of the process is dependent on the total number of surface-active receptors (Figure 5B).[45] By prolonging the period, another phase has been noticed that indicates the operation of different further mechanisms, such as the influence of RB diffusion activities and the layered adsorption chemical processes.[19,44] Finally, it was successfully established that the third phase prevails whenever the CA and PANI/C particulates are in their equilibrium states for the RB adsorption processes. This demonstrates that the sequestered RB molecules entirely occupied or filled all of the effective binding sites (Figure 5B).[16,43] The regulation of RB uptake behaviors during this phase is controlled by molecular interactions and/or interionic attraction.[46]

2.2.2.3. Kinetic Modeling. The kinetic properties of the uptake activities of RB by CA and PANI/C particulates are illustrated employing the well-established kinetic assumptions of the pseudo-first-order (P.F.) (Figure 5C) as well as pseudo-second-order (P.S.) (Figure 5D) models. The degree of agreement between the kinetic assumptions of two examined models and the measurable uptake behaviors of RB was computed using nonlinear fitting methods. This assessment was made based on both the R^2 value (correlation coefficient) and the chi-squared (χ^2) values. The obtained R^2 values, in conjunction with χ^2, suggest that the adsorption activities of RB by CA and PANI/C particulates exhibit better alignment with the kinetic properties and basic principles of the P.F. model compared to the examined P.S. model (Figure 5C,D and Table 1). The observed agreement between the experimentally verified capacities of CA and PANI/C under equilibrium conditions (111.3 mg/g for CA and 140.5 mg/g for PANI/C) and the corresponding values estimated mathematically (120.6 mg/g for CA and 148.7 mg/g for PANI/CA) supports these findings (Table 1). Based on the kinetic principles of the P.F. model, physical mechanisms were mainly responsible for the sequestration of RB by CA and PANI/C particulates. These mechanisms might have included significant impacts of the forces of van der Waals and/or electrostatic attraction.[47,48] Even though the P.F. model's formula for eliminating RB by CA and PANI/C particulates is more matched than the P.S. model's illustrated equation, the uptake behaviors maintain considerable agreement with the P.S. kinetic. Therefore, it was expected that a variety of common weak chemical processes, including hydrogen bonding, chemical complexation, electron sharing, and hydrophobic interactions, would play a subordinate role or possess a minor effect on the reactions.[43,47] The combined effects of the

https://doi.org/10.1021/acsomega.3c07355
ACS Omega 2023, 8, 47210−47223

Table 1. Mathematical Parameters of the Evaluated Kinetic Models

material	model	parameters	values
CA	pseudo-first-order	K_1 (1/min)	0.006
		$Qe_{(Cal)}$ (mg/g)	120.6
		R^2	0.95
		χ^2	1.98
	pseudo-second-order	k_2 (mg/g min)	3.2×10^{-5}
		$Qe_{(Cal)}$ (mg/g)	157.8
		R^2	0.918
		χ^2	3.12179
PANI/C	pseudo-first-order	K_1 (1/min)	0.0065
		$Qe_{(Cal)}$ (mg/g)	148.75
		R^2	0.97359
		χ^2	0.99137
	pseudo-second-order	k_2 (mg/g min)	3.034×10^{-5}
		$Qe_{(Cal)}$ (mg/g)	190
		R^2	0.94
		χ^2	2.07

two types of processes lead to the formation of a chemically adsorbed RB layer, which is then followed by the formation of a physically adsorbed layer using the earlier one as the foundation for it.[49]

2.2.3. Equilibrium Studies. 2.2.3.1. Effect of RB Concentrations. Within a testing range of 25 to 350 mg/L, the significance of the beginning examined RB levels on the adsorption properties of CA and PANI/C was established after systematically adjusting each of the influencing variables at particular values [time: 24 h; volume: 100 mL; solid dosage: 0.2 g/L; temperature: 298, 308, and 313 K; pH: 8]. Following the assessment of the adsorption properties of CA and PANI/C composites, the initial RB concentration serves as a significant parameter for elucidating the equilibrium behavior and maximum adsorption capacities. The quantity of RB that was adsorbed significantly increased after analyzing the properties of CA and PANI/C in the presence of a higher concentration of RB ions (Figure 6A,B). The presence of higher concentrations of RB within certain volumes induces a significant enhancement in the diffusion, mobility, and driving forces of the dye ions. Consequently, this leads to increased collisions alongside the chemical interactions with active sites that are distributed on the surfaces of CA and PANI/C. Therefore, the efficiency of the RB dye uptake has been enhanced.[43,46] The increase in RB-adsorbed quantities in comparison to the initial studied concentrations can be clearly observed up to the specified tested values (Figure 6A,B). Following that, an increase in the beginning RB concentrations displays overlooked effects on the adsorbed quantities of their molecules, either by CA or by PANI/C. These effects distinguish the equilibrium states and contribute to the establishment of the best adsorption values. The detection of the equilibrium of CA as an adsorbent may be noticed at various temperatures (298, 308, and 313 K) with maximal capacities of 252.8 230.6, and 201.5 mg/g, respectively (Figure 6A). In comparison, the reported values for PANI/C are 420.5 390.3, and 341.7 mg/g at the same temperatures (Figure 6B). The enhanced efficiency of PANI/C in removing RB compared to CA-free particulates can be assigned to several factors. First, the integration of PA leads to an elevated surface area, facilitating effective adsorption of more RB molecules. Second, the total quantity of active sites is significantly

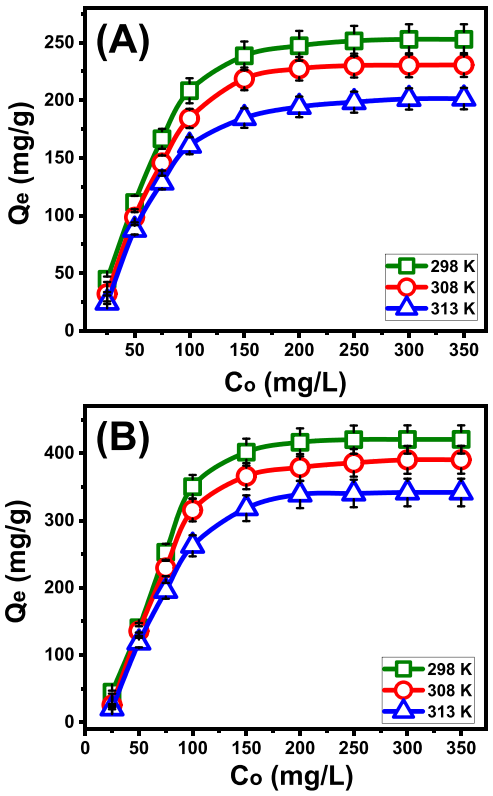

Figure 6. Influence of the RB starting concentrations on the uptake capacities of CA (A) and PANI/C (B).

increased after the incorporation of PANI, further enhancing the removal capacity of the composite. Last, the organophilicity of the composite is significantly improved, contributing to its enhanced uptake qualifications. The reduction in the adsorption of RB by CA and PANI/C as the temperature increased suggests that the processes were exothermic.

2.2.3.2. Giles's Classification. The RB isotherm curves using CA and PANI/C were categorized based on Giles classification guidelines. The analysis verified that these curves exhibited an L-type equilibrium (Figure 6A,B). The equilibrium qualities of the L-type reflect the notable and influential effects of intermolecular attraction forces during the adsorption mechanisms of RB by the CA and PANI/C particulates. These effects are further intensified by the powerful interactions between the RB molecules and the chemically reactive frameworks of the CA and PANI/C particulates.[50] On the basis of L-type isotherm features, it was also possible to forecast a complete formation of adsorbed RB monolayers onto the exterior surfaces of CA and PANI/C particulates.[51] Moreover, the observed isothermal behavior implies the presence of active free as well as active receptors throughout the CA and PANI/C particulates, which display significant selectivity toward RB molecules, especially at low initial concentrations.

2.2.3.3. Classic Isotherm Models. The equilibrium behaviors of the retention activities of RB by CA and PANI/C particulates were described based on the concepts of the classic Langmuir (Figure 7A−C), Freundlich (Figure 7D−F), and Dubinin−Radushkevich (D−R) (Figure 7G−I) models. The assessment of the agreement between the equilibrium theories of all the models and RB uptake activities was conducted based on the nonlinear fit levels with their corresponding formulas

https://doi.org/10.1021/acsomega.3c07355
ACS Omega 2023, 8, 47210−47223

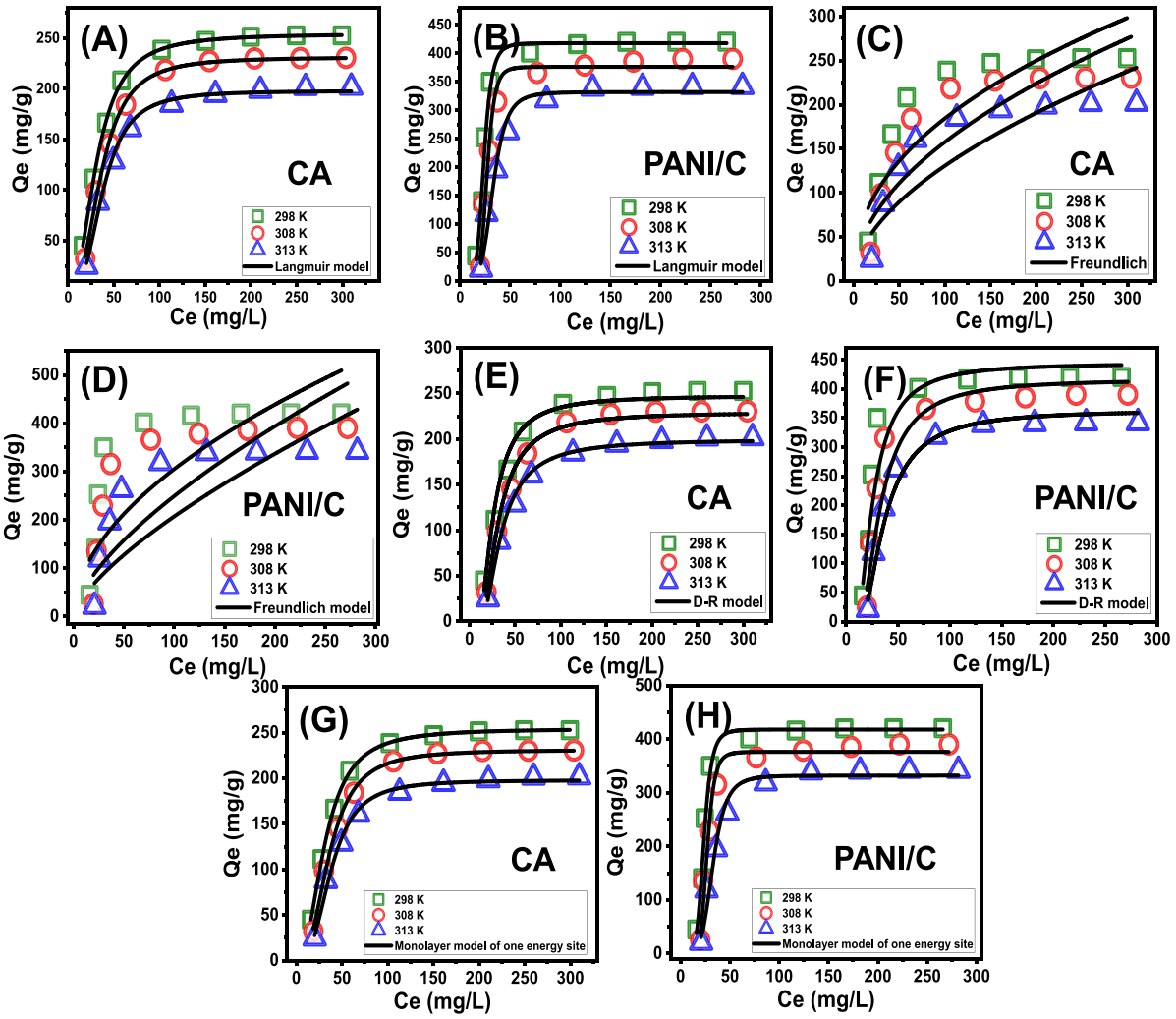

Figure 7. Fitting of the RB uptake results of CA and PANI/C with the classic and advanced equilibrium models including the Langmuir model (A, B), Freundlich model (C, D), D−R model (E, F), and advanced monolayer model of one energy site (G, H).

for all of them, which were dependent on the numerical values of the R^2 (correlation coefficient) and chi-squared (χ^2). The R^2 and χ^2 values indicate that the RB uptake behaviors of the CA and PANI/C particulates align more closely with the Langmuir isotherm fundamentals (Figure 7 and Table 2) instead of the basic features of the Freundlich isotherm (Figure 7 and Table 2). The Langmuir isotherm depicts the homogeneous adsorption of RB on the empty and active sites of CA and PANI/C particulates in monolayer arrangements.[47,48] Moreover, the calculated RL values for the absorption activities of RB by CA and PANI/C particulates are below 1, suggesting that these reactions exhibit favorable characteristics.[16,45] The supposed maximum adsorption capacities (Q_{max}) of CA for RB are 254.4 mg/g (298 K), 231.2 mg/g (308 K), and 204.1 mg/g (313 K). Conversely, the calculated values for PANI/C are 427.9 mg/g (298 K), 396.3 mg/g (308 K), and 345.05 mg/g (313 K).

The D−R model's isotherm concepts (Figure 7 J−L) provide an explanation for the energy changes of the CA and PANI/C particulates during the uptake testing of RB, regardless of the homogeneous or heterogeneous nature of their surfaces.[52] The mathematical parameters, such as Gaussian energy (E), play a vital role when estimating the type of RB uptake mechanisms that impact it, whether they are of a chemical or physical nature. Adsorption processes with E values of 8, 8−16, and > 16 kJ/mol reflect the effects of highly physical, poor chemical and/or complicated physical/chemical, and powerful chemical mechanisms, respectively.[16,52] The recorded values of the E parameter for the RB absorption activities of CA and PANI/C fall within the suggested energy ranges of physical reactions (<8 kJ/mol), consistent with the findings of the theoretical analysis of the kinetic examination (Table 2).

2.2.3.4. Advanced Isotherm Modeling. The investigation of advanced equilibrium mathematical models in accordance with the principles of statistical physics hypotheses can provide valuable insights into the distinctive features of adsorption processes, particularly in relation to the interfaces between adsorbents and adsorbates as well as the surface properties of solid adsorbents. The mathematical parameters obtained from these models, including the energetic and steric sections, have the potential to be used to highlight the mechanistic activities. The steric aspects encompassed various parameters, such as the number of filled functional sites of CA and PANI/C by RB ($N_{m(RB)}$), the overall number of RB molecules that have been occupied at each site ($n_{(RB)}$), and the adsorption capacities of CA and PANI/C under saturation conditions ($Q_{sat(RB)}$) (Table 3). The energetic parameters considered in this study included

https://doi.org/10.1021/acsomega.3c07355
ACS Omega 2023, 8, 47210−47223

Table 2. Mathematical Parameters of the Evaluated Classic Isotherm Models

materials	models	parameters	298 K	308 K	313 K
CA	Langmuir model	Q_{max} (mg/g)	254.3	231.2	204.11
		b (L/mg)	3.43×10^{-4}	8.7×10^{-5}	3.28×10^{-5}
		R^2	0.99	0.99	0.99
		χ^2	0.19	0.21	0.4
	Freundlich model	$1/n$	0.44	0.508	0.55
		k_F (mg/g)	24.43	15.21	10.6
		R^2	0.792	0.784	0.79
		χ^2	5.12	6.2	3.58
	D−R model	β (mol^2/kJ^2)	0.072	0.041	0.036
		Q_m (mg/g)	247.73	229.45	199.68
		R^2	0.98	0.99	0.99
		χ^2	0.96	0.406	0.15
		E (kJ/mol)	2.63	3.49	3.72
PANI/C	Langmuir model	Q_{max} (mg/g)	427.9	396.3	345.05
		b (L/mg)	6.9×10^{-9}	4.7×10^{-11}	2.29×10^{-8}
		R^2	0.99	0.98	0.98
		χ^2	1.82	4.3	3.38
	Freundlich model	$1/n$	0.52	0.66	0.7
		k_F (mg/g)	27.29	11.93	8.17
		R^2	0.66	0.64	0.688
		χ^2	51.17	62.9	49.8
	D−R model	β (mol^2/kJ^2)	0.016	0.028	0.031
		Q_m (mg/g)	444.3	416.82	363.494
		R^2	0.98	0.92	0.97
		χ^2	3.3	4.7	4.69
		E (kJ/mol)	5.59	4.22	4.01

Table 3. Estimated Mathematical Parameters for the Fitting Process with Monolayer Model of One Energy

		n	N_m (mg/g)	Q_{sat} (mg/g)	C1/2 (mg/L)	ΔE (kJ/mol)
CA	298 K	2.32	109.617	254.31	31.12	−4.36
	308 K	2.609	88.64	231.26	36.03	−4.85
	313 K	2.85	70.62	202.1	38.115	−5.06
PANI/C	298 K	5.98	70.83	423.56	23.581	−4.68
	308 K	7.2	54.5	392.4	26.89	−4.34
	313 K	5.05	67.97	343.24	32.93	−4.65

the adsorption energy of RB (ΔE), internal energy (E_{int}), free enthalpy (ΔG), and entropy (Sa). A simulation of RB uptake processes has been conducted employing nonlinear fits with the model's descriptive equations. The achievement of this objective has been performed by multivariable nonlinear regression analysis and the application of the Levenberg−Marquardt iterating approach. The adsorption operations of RB by CA and PANI/C were represented using a monolayer model consisting of a single energy site, considering the fitting degrees of the results with the model (Figure 7G,H and Table 3).

Steric Properties: Number of Adsorbed RB (n) per Each Site. The numerical results of the $n_{(RB)}$ parameter strongly indicate the orientation that occurred when the RB molecules were adsorbed on the outermost surfaces of CA and PANI/C, whether it was vertical or horizontal. These values also provide insights into the mechanistic processes involved, specifically whether the adsorption involved multiple dockings or multiple interactions. The mechanisms that are most affected by multianchorage or multidocking mechanisms include the uptake of a single RB molecule by several uptake sites in horizontal arrangements. Therefore, the n parameter of the retention processes exhibits a value smaller than 1. On the other hand, systems exhibiting values greater than 1 exhibit both nonparallel and vertical arrangements for the adsorbed RB. This suggests that the uptake activities in these systems are primarily caused by multi-ionic processes, which involve the adsorption of multiple dye molecules on a single site.[16,53] The calculated values of n during the uptake of RB ($n_{(RB)}$ = 2.32−2.85 for CA; $n_{(RB)}$ = 5.05−7.2 for PANI/C) exhibit values above 1 (Figure 8A and Table 3). Consequently, the RB molecules had been taken up by multimolecular mechanisms. In this process, each uptake site on the structure of the CA and PANI/C materials had the capacity to receive several RB molecules in a vertical orientation and had nonparallel characteristics. Whereas each site of CA may retain up to three molecules of RB, each site on PANI/ZA can absorb up to eight molecules, indicating an increase in the selectivity of the receptor sites toward the cationic RB molecules following PA integration.

Regarding the effects of temperature, the determined $n_{(RB)}$ values of CA verify that they are increased with raising the temperature from 298 to 313 K (Figure 8A and Table 3). This is often ascribed to the supposed enhancement in the aggregation properties of RB when it is adsorbed by CA at higher temperatures.[54] Furthermore, the aforementioned observation demonstrates the existence of thermal activation mechanisms that occur before the capture of RB by CA.[2,55] In the case of the PANI/C composite, the incorporation of PA has an extensive effect on the reported behaviors. When the test temperature was raised from 298 to 308 K, the $n_{(RB)}$ values rose dramatically. However, when the test temperature was increased to 313 K, they fell once again (Figure 8A and Table 3). The observed behavior can potentially be attributed to changes in the quantity and types of functional receptors of RB

https://doi.org/10.1021/acsomega.3c07355
ACS Omega 2023, 8, 47210−47223

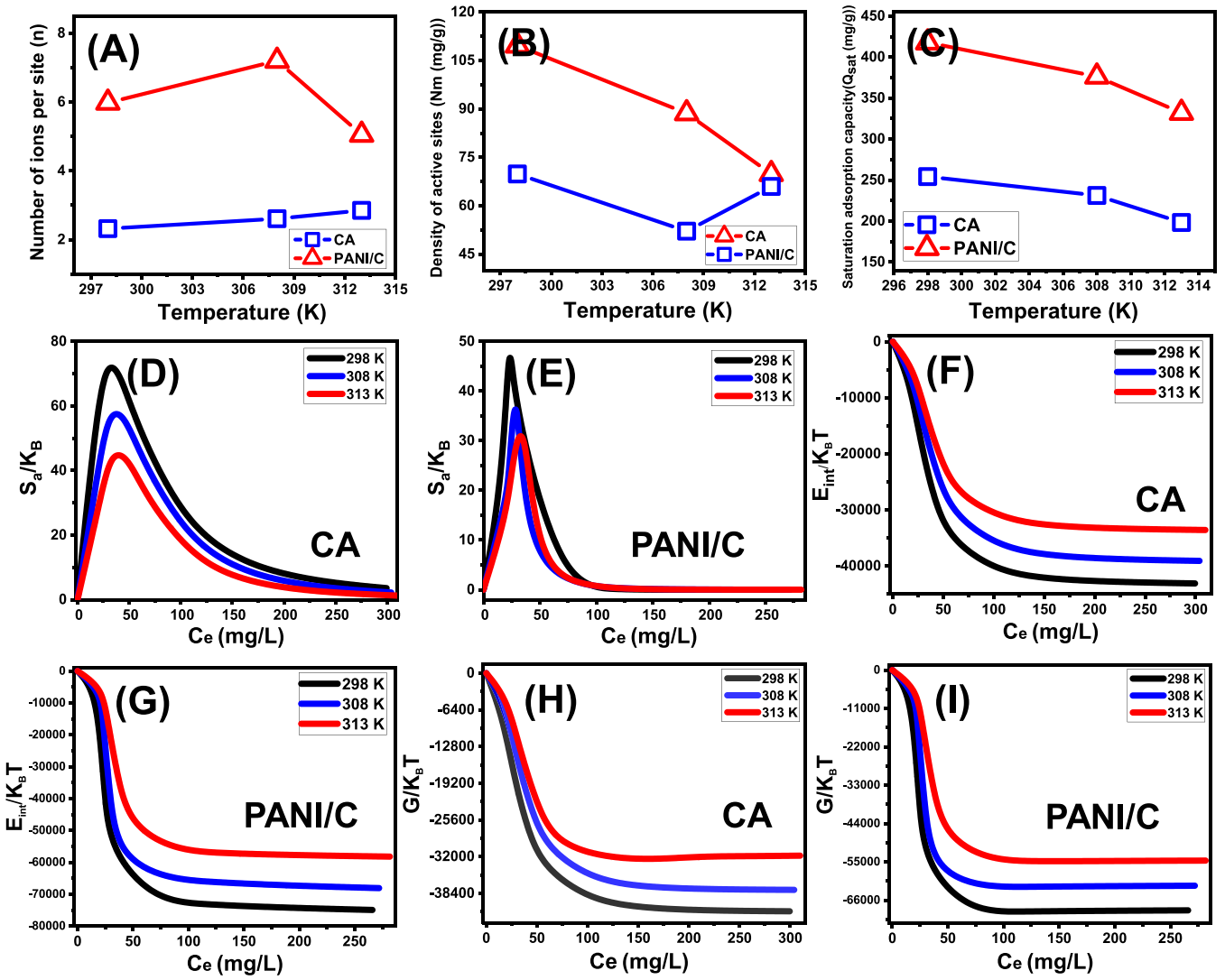

Figure 8. Changes in the number of adsorbed RB molecules per each active site (A), active site density of CA and PANI/C (B), RB adsorption capacity at saturation states (C), entropy properties during the uptake of RB (D, E), internal energy properties during the uptake of RB (F, G), and enthalpy properties (H, I).

molecules with the variations in temperature conditions after the experimental integration of PA chains.[56,57]

Steric Properties: Occupied Active Site Density (N_m). The density of the RB-occupied sites ($N_{m(RB)}$) of CA and PANI/C substantially represents the total quantity of the free and efficient adsorption receptors across the exteriors of its nanoparticles during the reaction (Figure 8B and Table 3). CA has estimated $N_{m(RB)}$ values of 109.6 mg/g (298 K), 88.6 mg/g (308 K), and 70.88 mg/g (313 K) (Figure 8B and Table 3). In contrast with most of the previously studied hybrid structures, the integrated polymer PANI resulted in a decline in the quantities of the present active sites. The determined occupied active site densities (N_m) of PANI/C are 70.8 mg/g (298 K), 54.5 mg/g (308 K), and 67.9 mg/g (313 K) (Figure 8B and Table 3). This behavior is in agreement with the reported behaviors of $n_{(RB)}$ of PANI/C at the same conditions; the aggregation of RB molecules and the increase in the related $n_{(RB)}$ values are in reversible relation to the estimated quantities of the occupied active sites. Moreover, this demonstrates the impact of the integrated polymer in inducing the affinity of the formed composite by changing the exposed chemical groups rather than the textural impact. The $N_{m(RB)}$ values of both CA and PANI/C exhibit temperature-dependent reversible change in terms of their response to temperature variations (Figure 8B and Table 3). The observed values of $n_{(RB)}$ align with earlier findings since an increase in aggregation affinities leads to a reduction in the total number of occupied sites. Additionally, the temperature has an impact on the dominant state of the active sites.[2,58]

Steric Properties: Adsorption Capacity at the Saturation State of (Q_{sat}). CA and PANI/C RB adsorption efficiencies at saturation (Q_{sat}) reflect the best acceptable anticipated value for maximum absorption capabilities. The values of Q_{sat} are affected by two key variables: the established density of the filled sites (N_m) and the total quantity of adsorbed RB molecules per site (n). CA has calculated Q_{sat} values for RB as a prospective adsorbent of 254.3 mg/g (298 K), 231.2 mg/g (303 K), and 202.1 mg/g (313 K) (Figure 8C and Table 3). The use of the PANI/C composite maintains a significant increase in its adsorption qualities at saturation phases, specifically at 423.56 mg/g (298 K), 392.4 mg/g (308 K), and 343.2 mg/g (313 K) (Figure 8C and Table 3). The exothermic characteristics of RB uptake activities by CA and PANI/C are concluded from the adverse impact of the

https://doi.org/10.1021/acsomega.3c07355
ACS Omega 2023, 8, 47210−47223

temperature on the efficiency of the reactions (Figure 8C and Table 3). This further demonstrated the uptake temperature's promoting impact on thermal collisions, which results in a reduction in the RB adsorption's efficacy.[53] Moreover, the established Q_{sat} properties for raw coal (CA) with testing temperature confirm their influence by the mentioned behaviors of N_m rather than n, implying that the present active sites regulate the efficiency of adsorption rather than the capacity of each active site. Conversely, the PANI/C composite's adsorption efficiency is dependent on each site's adsorption capacity ($n_{(RB)}$) as well as the number of active sites ($N_{m(RB)}$).

Energetic Properties: Adsorption Energy. RB uptake reactions' energies (ΔE) may reliably reveal the nature of impacting mechanisms, whether they relate to physical or chemical processes. While physical processes possess energy levels below 40 kJ/mol, chemical pathways possess energy levels greater than 80 kJ/mol. The categorization of physically occurring mechanistic activities is based on the adsorption energy values. These types of interactions include coordinating exchange (40 kJ/mol), forces of dipole bonds (2−29 kJ/mol), hydrogen bonds (<30 kJ/mol), van der Waals force (4−10 kJ/mol), and hydrophobic bonds (5 kJ/mol).[54,59] The mathematical calculation of the RB uptake energies (ΔE) was performed using eq 1, which incorporates the solubility of RB in water (S), gas constant (R = 0.008314 kJ/mol·K), the RB concentrations during the half-saturation states of CA and PANI/C, and the absolute temperature (T).[57]

$$\Delta E = RT\ln\left(\frac{S}{C}\right) \tag{1}$$

The estimated energies for RB retention by CA and PANI/C fall within the ranges of −4.3 to −5.06 and −4.3 to −4.6 kJ/mol, respectively (Table 3). As a consequence, the predominant mechanisms that were associated with the uptake of RB by either CA or PANI/C could potentially be attributed to physical mechanisms, including van der Waals forces (4 to 10 kJ/mol), forces of dipole bonds (2 to 29 kJ/mol), and hydrogen bonds (<30 kJ/mol). Furthermore, the computed values of ΔE exhibit significant negative signals for both CA and PANI/C. These findings correlate with the preceding experimental results that demonstrated the exothermic nature of the uptake processes. Such energetic findings are in significant agreement with the previously reported adsorption mechanisms for coal as well as PA. It was reported that the uptake of dye by PA occurs mainly by hydrogen binding, electrostatic altercations, and pi−pi interaction.[25−27] For the adsorption mechanisms of coal, the previous studies demonstrated the uptake of the dyes by electrostatic attractions with the reactive chemical groups of coal, hydrogen bonding between the free hydrogen on the surface of coal and the nitrogen atoms of the dyes structure, and $\pi-\pi$ interactions that occur between the aromatic ring of the dye molecules and the coal structure, which is associated with dispersion in addition to dipole/dipole interactions.[17−19]

Energetic Properties: Thermodynamic Functions. (1) Entropy. The entropy (Sa) of the RB elimination activities by CA and PANI/C significantly demonstrates the order and disorder aspects of their surfaces, depending on the impact of different dye concentrations as well as the operating temperature of the investigated reactions. The characteristics of the Sa have been perceived by using the results obtained from eq 2, employing the previously established values of N_m and n, together with the determined RB concentrations beneath the half-saturation stages of CA and PANI/C (C1/2).

$$\frac{S_a}{K_B} = N_m\left\{\ln\left(1+\left(\frac{C}{C_{1/2}}\right)^n\right) - n\left(\frac{C}{C_{1/2}}\right)^n \frac{\ln\left(\frac{C}{C_{1/2}}\right)}{1+\left(\frac{C}{C_{1/2}}\right)^n}\right\} \tag{2}$$

Based on the displayed curves, it can be noticed that the entropy levels (Sa) exhibit a notable decrease during the uptake of RB by CA (Figure 8D) and PANI/C (Figure 8E) when subjected to tests conducted with elevated RB concentrations. The observed trend demonstrates a significant reduction in the disorder features of the surfaces of both CA and PANI/C as the measured RB concentrations increase. These entropy properties also support the effective docking of the RB inside the CA and PANI/C active and empty interaction sites in the context of low dye concentrations.[57,58] Entropy maximal values for CA were noted at RB equilibrium levels of 27.7 mg/L (313 K), 30.28 mg/L (308 K), and 32.4 mg/L (298 K) (Figure 8D). The equilibrium levels of maximum entropy for the uptake of RB by PANI/C were found to be 24.29 mg/L at 298 K, 29.12 mg/L at 308 K, and 35.9 mg/L at 313 K (Figure 8E). The equilibrium levels observed in the present investigation exhibit a notable resemblance to the concentrations estimated at the half-saturation phases of CA and PANI/C. In turn, this prevents more RB ions from docking onto their remaining empty receptors. Furthermore, the significant reductions observed in the calculated entropy values indicate a substantial drop in the number of available sites and a notable decline in the freedom and mobility properties of the RB ions.[60,61]

(2) Internal Energy and Free Enthalpy. The internal energy (E_{int}) that corresponds to RB uptake operations by CA and PANI/C beside the free enthalpy (ΔG) properties, considering the experimental changes in the dye concentration and operating temperature, have been assessed using values obtained from eqs 3 and 4, respectively, according to previously established N_m, n, and C1/2, as well as the translation partition (Z_v).[55]

$$\frac{E_{int}}{K_B T} = nN_m\left[\left(\frac{\left(\frac{C}{C_{1/2}}\right)^n \ln\left(\frac{C}{Z_v}\right)}{1+\left(\frac{C}{C_{1/2}}\right)^n}\right) - \left(\frac{n\ln\left(\frac{C}{C_{1/2}}\right)\left(\frac{C}{C_{1/2}}\right)^n}{1+\left(\frac{C}{C_{1/2}}\right)^n}\right)\right] \tag{3}$$

$$\frac{G}{K_B T} = nN_m \frac{\ln\left(\frac{C}{Z_v}\right)}{1+\left(\frac{C_{1/2}}{C}\right)^n} \tag{4}$$

The calculated internal energy (E_{int}) quantities for the conducted RB uptake experiments using CA (Figure 8F,G) and PANI/C (Figure 8H,I) show negative values. These findings demonstrate a significant decrease in E_{int} once the temperature increases from 298 to 313 K. This observation serves to strengthen the spontaneous and exothermic nature of the RB adsorption processes mediated by both CA and PANI/C. Regarding the established enthalpy values, the same behaviors and characteristics have been recognized. The G values display a negative sign and demonstrate a reversible correlation with the testing temperature. This suggests a

https://doi.org/10.1021/acsomega.3c07355
ACS Omega 2023, 8, 47210−47223

decrease in the feasibility properties and confirms the spontaneity and exothermic nature of the RB uptake by both CA and PANI/C composites.

2.2.4. RECYCLABILITY

The recyclable potential of the PANI/C composite as an adsorbent of the RB dye was investigated as an important factor throughout the product evaluation for both industrial and practical applications. The used PANI/C particles had been thoroughly rinsed with distilled water for 10 min, and this process was performed five times. The cleaned PANI/C was subsequently dried at 60 °C for 8 h so it could be further utilized in other RB adsorption cycles. The implemented recyclability experiments were carried out by keeping the factors of adsorption at pH 8 for 0.20 g/L (PANI/C dosage), 24 h (duration), 200 mL (volume), 50 mg/L (RB concentrations), and 298 K (temperature). In light of the five runs that had been performed to test recyclability, the obtained RB adsorption effectiveness employing PANI/C as the adsorbent exhibits notable stability and excellent recyclability characteristics. Recyclability of PANI/C led to an adsorption effectiveness of 140.5 mg/g (cycle 1), 137.2 mg/g (cycle 2), 131.8 mg/g (cycle 3), 1 mg/g (cycle 4), and 123.6 mg/g (cycle 5).

The previously reported high recyclability properties, in addition to the high adsorption capacity of RB dye, operation pH range, facile production procedures, low fabrication cost, high natural availability, and eco-friendly value, strongly recommend that the synthetic PANI/C composite be applied effectively in realistic purification of wastewater from synthetic dyes such as RB dye.

3. CONCLUSIONS

The adsorption of RB dye by a synthetic PANI/C hybrid was evaluated based on the synergetic-enhancing influence of the PANI polymers on its uptake properties. The PANI/C blend exhibited a significant improvement in uptake qualities with a value of 423.5 mg/g in comparison to CA, which had a value of 254.3 mg/g. The adsorption behaviors of RB by PANI/C, as well as the mechanisms that regulate these behaviors, were assessed by employing the hypotheses of the traditional Langmuir isotherm and the advanced monolayer model with one site of energy. The incorporation of PANI induces the capacities of the present active sites rather than their quantities, which induce the uptake properties of the composite. Each single site on PANI/C can adsorb about eight molecules of RB as compared to three for natural coal. This also implies a vertical arrangement for the adsorbed dye and the operation of multimolecular mechanisms. The measured values of the adsorption energies of RB, which are less than 40 kJ/mol, in conjunction with the thermodynamic functions indicate that the elimination of RB occurs by exothermic, physical, and spontaneous mechanisms.

4. EXPERIMENTAL WORK

4.1. Materials. A low- to medium-grade form of volatile subbituminous coal was employed in the production of the assessed adsorbents, and it was purchased locally from the El-Maghara raw coal mines in Sinai, Egypt. On the basis of the findings from the ultimate-proximate chemical investigations, the initial composition and the primary elemental composition of the assessed raw coal specimen were determined and are displayed in Table 1. The aniline monomers (C_6H_7N), sodium hydroxide pellet (NaOH), methanol, ammonium persulfate ($(NH_4)_2S_2O_8$), hydrochloric acid (HCl), and ethanol employed for the composite's fabrication were purchased from Sigma-Aldrich Company in Egypt. During the adsorption studies, RB dye ($C_{28}H_{30}N_2O_3$) (97% dye content; MW: 479.029 g/mol; Sigma-Aldrich) was used as the dye pollution source. During the studies, pH adjusters included sodium hydroxide solution (0.1 M) and diluted nitric acid (0.1 M).

4.2. Synthesis of Polyaniline/Coal Nanocomposite (PANI/C). The coal fractions and PA polymer have been blended according to the method reported by Sayed et al.[29] An aniline solution was produced by mixing dilute hydrochloric acid (0.5M) with the aniline monomers (0.1 M) under the impact of ultrasonic vibrations. Following that, employing cooperative mixing systems comprising magnetic stirring and an ultrasonic source, we evenly distributed the powdered coal fractions (1 g) throughout the aniline solutions. The oxidizing chemical reagent $(NH_4)_2S_2O_8$ (0.15 M) was incorporated into the mixture instantaneously, and it was then constantly agitated for 24 h to facilitate the polymerization procedure considering the formation pH at pH 2. The developed composite was then separated (15 min; 3000 rpm) by centrifuging, carefully cleaned, and subsequently left to dry overnight at 50 °C. The composite particulates were then marked with PANI/C and kept for further analysis and dye adsorption activities.

4.3. Analytical Techniques. The crystalline states and crystalline properties of the materials were investigated and evaluated by utilizing a PANalytical-Empyrean X-ray diffractometer within a measuring range of 0 to 70°. Employing a Fourier transform infrared spectrometer (FTIR-8400S; Shimadzu) within a wavelength range of 400 to 4000 cm^{-1}, the changes in the functional chemical structures through the production procedures have been detected. Following the coating stage for the powdered composite by a thin film of gold, the morphologies were determined based on the recognized images that have been captured by SEM (Gemini, Zeiss Ultra 55). HRTEM images acquired using a transmission electron microscope (JEOL JEM-2100) at an acceleration voltage of 200 kV were used as well for assessing the internal characteristics of the established composite. After carefully degassing the materials, their porosity and specific surface area were determined using a surface area analyzer (Beckman Coulter SA3100) considering the ensuing N_2 adsorption/desorption isotherms.

4.4. Batch Adsorption Studies of RB Dye. RB dye was adsorbed by PANI/C employing normal adsorption parameters of pH (3−10), contact time (30−840 min), and RB concentration (25−350 mg/L) at a range of temperatures (25−40 °C). This was performed by keeping the other influencing factors at certain values (0.2 g/L of PANI/C (dosage) and 100 mL (RB volume)). The experiments were carried out three times, and the mean results of established RB absorption capacities with a standard deviation of 3.4% were utilized throughout the analysis of the outcomes. The RB adsorption capacities have been established by measuring the residual RB concentrations in the treated solutions utilizing a UV−vis spectrophotometer at an adjustable wavelength of 554 nm in accordance with eq 5.

$$Q_{e(mg/g)} = \frac{(C_o - C_e)V}{m} \quad (5)$$

https://doi.org/10.1021/acsomega.3c07355
ACS Omega 2023, 8, 47210−47223

The symbols Q_e (mg/g), C_e (mg/L), C_o (mg/L), m (mg), and V (mL) represent the determined RB adsorption performance, remaining RB concentration, beginning RB concentration, PANI/C amounts, and volume of the RB solutions, respectively. The frequently used traditional isotherm models were used to illustrate the equilibrium properties of the RB uptake activities based on the fundamental fitting parameters including the correlation coefficient (R^2) (eq 6) and chi-square (χ^2) (eq 7). The fitting values for the advanced equilibrium models established in accordance with the statistical physics hypothesis (Table S1) were assessed using R^2 and the root mean square error (RMSE) (eq 8). This was performed using the estimated values for $Q_{e,exp}$ (experimental uptake capacities) and $Q_{e,cal}$ (theoretical uptake capacities) as well as m' (the verified end outcomes) and p (experimental variables).

$$R^2 = 1 - \frac{\sum (Q_{e,exp} - Q_{e,cal})^2}{\sum (Q_{e,exp} - Q_{e,mean})^2} \quad (6)$$

$$\chi^2 = \sum \frac{(Q_{e,exp} - Q_{e,cal})^2}{Q_{e,cal}} \quad (7)$$

$$RMSE = \sqrt{\frac{\sum_{i=1}^{m} (Q_{e,cal} - Q_{e,exp})^2}{m' - p}} \quad (8)$$

■ ASSOCIATED CONTENT

Supporting Information

The Supporting Information is available free of charge at https://pubs.acs.org/doi/10.1021/acsomega.3c07355.

Representative equations of the kinetic and isotherm models (Table S1) and the SEM image of free polyaniline particles (Figure S1) (PDF)

■ AUTHOR INFORMATION

Corresponding Authors

Wail Al Zoubi − *Materials Electrochemistry Laboratory, School of Materials Science and Engineering, Yeungnam University, Gyeongsan 38541, Republic of Korea;* orcid.org/0000-0003-4213-8481; Email: wailalzoubi@ynu.ac.kr

Mostafa R. Abukhadra − *Materials Technologies and their Applications Lab, Geology Department, Faculty of Science, Beni-Suef University, Beni Suef City, Egypt; Geology Department, Faculty of Science, Beni-Suef University, Beni Suef 62521, Egypt;* orcid.org/0000-0001-5404-7996; Email: Abukhadra89@Scinec.bsu.edu.eg

Authors

Mohamed Adel Sayed − *Materials Technologies and their Applications Lab, Geology Department, Faculty of Science, Beni-Suef University, Beni Suef City, Egypt; Department of Chemistry, Faculty of Science, Beni-Suef University, 62514 Beni Suef City, Egypt*

Abdelrahman Mohamed − *Department of Chemistry, Faculty of Science, Beni-Suef University, 62514 Beni Suef City, Egypt*

Sayed A. Ahmed − *Department of Chemistry, Faculty of Science, Beni-Suef University, 62514 Beni Suef City, Egypt; Basic Science Department, Faculty of Engineering, Nahda University, Beni Suef 62764, Egypt*

Ahmed M. El-Sherbeeny − *Industrial Engineering Department, College of Engineering, King Saud University, Riyadh 11421, Saudi Arabia;* orcid.org/0000-0003-3559-6249

Complete contact information is available at: https://pubs.acs.org/10.1021/acsomega.3c07355

Author Contributions

This article was written through the contributions of all authors. All authors have given approval to the final version of the manuscript

Notes

The authors declare no competing financial interest.

Further studies will be conducted to follow the adsorption properties of the synthetic structures for different species of organic contaminants in comparative studies, considering the competitive effect. Also, the impact of the integration process of polyaniline on the affinity and selectivity properties of the composite will be assessed in detail.

■ ACKNOWLEDGMENTS

This publication is funded through the United States Agency for International Development (USAID). The contents are the responsibility of the authors and do not necessarily reflect the views of USAID or the United States Government. Also, the authors extend their appreciation to King Saud University for funding this work through Researchers Supporting Project number (RSP2023R133), King Saud University, Riyadh, Saudi Arabia.

■ REFERENCES

(1) Sajid, M.; Sajid Jillani, S. M.; Baig, N.; Alhooshani, K. Layered Double Hydroxide-Modified Membranes for Water Treatment: Recent Advances and Prospects. *Chemosphere* **2022**, *287*, No. 132140.

(2) Yang, X.; Wang, J.; El-Sherbeeny, A. M.; AlHammadi, A. A.; Park, W.-H.; Abukhadra, M. R. Insight into the Adsorption and Oxidation Activity of a ZnO/Piezoelectric Quartz Core-Shell for Enhanced Decontamination of Ibuprofen: Steric, Energetic, and Oxidation Studies. *Chem. Eng. J.* **2022**, *431*, No. 134312.

(3) Adly, E. R.; Shaban, M. S.; El-Sherbeeny, A. M.; Al Zoubi, W.; Abukhadra, M. R. Enhanced Congo Red Adsorption and Photo-Fenton Oxidation over an Iron-Impeded Geopolymer from Ferruginous Kaolinite: Steric, Energetic, Oxidation, and Synergetic Studies. *ACS Omega* **2022**, *7* (35), 31218−31232.

(4) Salam, M. A.; Mokhtar, M.; Albukhari, S. M.; Baamer, D. F.; Palmisano, L.; Jaremko, M.; Abukhadra, M. R. Synthesis and Characterization of Green ZnO@polynaniline/Bentonite Tripartite Structure (G.Zn@PN/BE) as Adsorbent for As (V) Ions: Integration, Steric, and Energetic Properties. *Polymers* **2022**, *14* (12), 2329 DOI: 10.3390/polym14122329.

(5) Khojastehnezhad, A.; Moeinpour, F.; Jafari, M.; Shehab, M. K.; Samih ElDouhaibi, A.; El-Kaderi, H. M.; Siaj, M. Postsynthetic Modification of Core−Shell Magnetic Covalent Organic Frameworks for the Selective Removal of Mercury. *ACS Appl. Mater. Interfaces.* **2023**, *15*, 28476−28490.

(6) Taher, T.; Putra, R.; Rahayu Palapa, N.; Lesbani, A. Preparation of Magnetite-Nanoparticle-Decorated NiFe Layered Double Hydroxide and Its Adsorption Performance for Congo Red Dye Removal. *Chem. Phys. Lett.* **2021**, *777*. 138712

(7) Okasha, A. T.; Abdel-Khalek, A. A.; El-Sherbeeny, A. M.; Zoubi, W. Al; Abukhadra, M. R. Advanced Equilibrium Study on the Synthesis and Characterization of Mg-Doped Hydroxyapatite Nano-Fibers as a Potential Enhanced Adsorbent of Zn (II) and Malachite Green Dye. *Mater. Today Commun.* **2023**, *35*, No. 105883.

(8) Pathania, D.; Dhar, S.; Sharma, A.; Srivastava, A. K. Decolourization of Noxious Safranin-T from Waste Water Using Mangifera Indica as Precursor. *Environmental Sustainability.* **2021**, *4*, 355−364.
(9) Abukhadra, M. R.; Mostafa, M.; El-Sherbeeny, A. M.; El-Meligy, M. A.; Nadeem, A. Instantaneous Adsorption of Synthetic Dyes from an Aqueous Environment Using Kaolinite Nanotubes: Equilibrium and Thermodynamic Studies. *ACS Omega* **2021**, *6* (1), 845−856.
(10) Spessato, L.; Duarte, V. A.; Viero, P.; Zanella, H.; Fonseca, J. M.; Arroyo, P. A.; Almeida, V. C. Optimization of Sibipiruna Activated Carbon Preparation by Simplex-Centroid Mixture Design for Simultaneous Adsorption of Rhodamine B and Metformin. *J. Hazard. Mater.* **2021**, *411*, No. 125166.
(11) Huang, Y.; Zheng, X.; Feng, S.; Guo, Z.; Liang, S. Enhancement of Rhodamine B Removal by Modifying Activated Carbon Developed from Lythrum Salicaria L. with Pyruvic Acid. *Colloids Surfaces A Physicochem. Eng. Asp.* **2016**, *489*, 154−162.
(12) Yuan, K.; Jiang, L.; Xing, Y.; Zhang, J.; Zhang, J.; Ye, X.; Ma, G.; Song, S.; Liu, C. Facile Synthesis and Study of Functional Porous Organic Polyaminals with Ultrahigh Adsorption Capacities and Fast Removal Rate for Rhodamine B Dye. *Microporous Mesoporous Mater.* **2022**, *344*, No. 112234.
(13) Gharbani, P.; Mehrizad, A. Preparation and Characterization of Graphitic Carbon Nitrides/Polyvinylidene Fluoride Adsorptive Membrane Modified with Chitosan for Rhodamine B Dye Removal from Water: Adsorption Isotherms. *Kinetics and Thermodynamics. Carbohydr. Polym.* **2022**, *277*, No. 118860.
(14) El Hassani, A. A.; Tanji, K.; El Mrabet, I.; Fahoul, Y.; El Gaidoumi, A.; Benjelloun, A. T.; Sfaira, M.; Zaitan, H.; Kherbeche, A. A Combined Molecular Dynamics Simulation, DFT Calculations, and Experimental Study of the Adsorption of Rhodamine B Dye on Kaolinite and Hydroxyapatite in Aqueous Solutions. *Surfaces and Interfaces* **2023**, *36*, No. 102647.
(15) Pandey, D.; Daverey, A.; Dutta, K.; Yata, V. K.; Arunachalam, K. Valorization of Waste Pine Needle Biomass into Biosorbents for the Removal of Methylene Blue Dye from Water: Kinetics, Equilibrium and Thermodynamics Study. *Environ. Technol. Innov.* **2022**, *25*, No. 102200.
(16) Sayed, I. R.; Farhan, A. M.; AlHammadi, A. A.; El-Sayed, M. I.; Abd El-Gaied, I. M.; El-Sherbeeny, A. M.; Al Zoubi, W.; Ko, Y. G.; Abukhadra, M. R. Synthesis of Novel Nanoporous Zinc Phosphate/Hydroxyapatite Nano-Rods (ZPh/HPANRs) Core/Shell for Enhanced Adsorption of Ni2+ and Co2+ Ions: Characterization and Application. *J. Mol. Liq.* **2022**, *360*, No. 119527.
(17) Al-Labadi, I. G.; Shemy, M. H.; Ghidan, A. Y.; Allam, A. A.; Kálmán, H. M.; Ajarem, J. S.; Luo, J.; Wang, C.; Abukhadra, M. R. Insight into the effects of H_2SO_4 and HNO_3 acidification processes on the properties of coal as an enhanced adsorbent for ciprofloxacin residuals: Steric and energetic studies. *Front. Chem.* **2023**, *11*, 1130682 DOI: 10.3389/fchem.2023.1130682.
(18) Al-Labadi, I. G.; Shemy, M. H.; Ghidan, A. Y.; Allam, A. A.; Kálmán, H. M.; Ajarem, J. S.; Luo, J.; Wang, C.; Abukhadra, M. R. Insight into the Effects of H2SO4 and HNO3 Acidification Processes on the Properties of Coal as an Enhanced Adsorbent for Ciprofloxacin Residuals: Steric and Energetic Studies. *Front. Chem.* **2023**, *11*, 1130682 DOI: 10.3389/fchem.2023.1130682.
(19) Surip, S. N.; Abdulhameed, A. S.; Garba, Z. N.; Syed-Hassan, S. S. A.; Ismail, K.; Jawad, A. H. H2SO4-Treated Malaysian Low Rank Coal for Methylene Blue Dye Decolourization and Cod Reduction: Optimization of Adsorption and Mechanism Study. *Surfaces and Interfaces* **2020**, *21*, No. 100641.
(20) Abukhadra, M. R.; Shemy, M. H.; El-Sherbeeny, A. M.; Soliman, A. T. A.; Zoubi, W. Al. Characterization of Sulfonated Raw Coal Products as Enhanced Adsorbents for Toxic Methyl Parathion Pesticide: Advanced Equilibrium Investigation and Effect of Acid Concentration. *Chem. Eng. Process. - Process Intensif.* **2022**, *182*, No. 109172.
(21) Flores, K. P.; Omega, J. L. O.; Cabatingan, L. K.; Go, A. W.; Agapay, R. C.; Ju, Y. H. Simultaneously Carbonized and Sulfonated Sugarcane Bagasse as Solid Acid Catalyst for the Esterification of Oleic Acid with Methanol. *Renew. Energy* **2019**, *130*, 510−523.
(22) Fonseca, J. M.; Spessato, L.; Cazetta, A. L.; Bedin, K. C.; Melo, S. A. R.; Souza, F. L.; Almeida, V. C. Optimization of Sulfonation Process for the Development of Carbon-Based Catalyst from Crambe Meal via Response Surface Methodology. *Energy Convers. Manag.* **2020**, *217*. 112975.
(23) Dutta, A.; Nirmale, A.; Nayak, R.; Selvakumar, M.; Bhat, S.; Paramasivam, S.; Senthil Kumar, S. Geometric Design Optimization of Polyaniline/Graphite Nanocomposite Based Flexible Humidity Sensor for Contactless Sensing and Breath Monitoring. *Mater. Lett.* **2022**, *323*, No. 132577.
(24) Zhao, Y.; Tian, S.; Lin, D.; Zhang, Z.; Li, G. Functional Anti-Corrosive and Anti-Bacterial Surface Coatings Based on Cuprous Oxide/Polyaniline Microcomposites. *Mater. Des.* **2022**, *216*, No. 110589.
(25) Abukhadra, M. R.; Saad, I.; Othman, S. I.; Katowah, D. F.; Ajarem, J. S.; Alqarni, S. A.; Allam, A. A.; Al Zoubi, W.; Gun Ko, Y. Characterization of Fe0@Chitosan/Cellulose Structure as Effective Green Adsorbent for Methyl Parathion, Malachite Green, and Levofloxacin Removal: Experimental and Theoretical Studies. *J. Mol. Liq.* **2022**, *368*, No. 120730.
(26) Meena, P. L.; Saini, J. K.; Surela, A. K.; Poswal, K.; Chhachhia, L. K. Fabrication of Polyaniline-Coated Porous and Fibrous Nanocomposite with Granular Morphology Using Tea Waste Carbon for Effective Removal of Rhodamine B Dye from Water Samples. *Biomass Convers. Biorefin.* **2022**, 1−20, DOI: 10.1007/s13399-021-02267-2.
(27) Minisy, I. M.; Salahuddin, N. A.; Ayad, M. M. Adsorption of Methylene Blue onto Chitosan−Montmorillonite/Polyaniline Nanocomposite. *Appl. Clay Sci.* **2021**, *203*, No. 105993.
(28) Duhan, M.; Kaur, R. Phytic Acid Doped Polyaniline Nanofibers: An Advanced Adsorbent for Methylene Blue Dye. *Environ. Nanotechnology, Monit. Manag.* **2019**, *12*, No. 100248.
(29) Singh, N. B.; Agarwal, A.; Rachna, K. Adsorptive and Photocatalytic Removal of Rhodamine B Dye from Water by Using Copper Ferrite Polyaniline Nanocomposite. *J. Sci. Ind. Res.* **2020**, *79*, 558−561.
(30) Sayed, M. A.; Abukhadra, M. R.; Salam, M. A.; Yakout, S. M.; Abdeltawab, A. A.; Aziz, I. M. Photocatalytic Hydrogen Generation from Raw Water Using Zeolite/Polyaniline@Ni2O3 Nanocomposite as a Novel Photo-Electrode. *Energy* **2019**, *187*, No. 115943.
(31) Jiao, W.; Ding, G.; Wang, L.; Liu, Y.; Zhan, T. Polyaniline Functionalized CoAl-Layered Double Hydroxide Nanosheets as a Platform for the Electrochemical Detection of Carbaryl and Isoprocarb. *Microchim. Acta* **2022**, *189* (2), 78.
(32) Abukhadra, M. R.; Bakry, B. M.; Adlii, A.; Yakout, S. M.; El-Zaidy, M. A. Facile Conversion of Kaolinite into Clay Nanotubes (KNTs) of Enhanced Adsorption Properties for Toxic Heavy Metals (Zn2+, Cd2+, Pb2+, and Cr6+) from Water. *J. Hazard. Mater.* **2019**, *374*, 296−308.
(33) Yu, H.; Niu, S.; Bai, T.; Tang, X.; Lu, C. Microwave-Assisted Preparation of Coal-Based Heterogeneous Acid Catalyst and Its Catalytic Performance in Esterification. *J. Clean. Prod.* **2018**, *183*, 67−76.
(34) Boral, P.; Varma, A. K.; Maity, S. Nitration of Jharia Basin Coals, India: A Study of Structural Modifications by XRD and FTIR Techniques. *Int. J. Coal Sci. Technol.* **2021**, *8* (5), 1034−1053.
(35) Abukhadra, M. R.; Saad, I.; Khim, J. S.; Ajarem, J. S.; Allam, A. A. Enhanced Oxidation of Antibiotic Residuals (Levofloxacin) Using a Green Composite of ZnO@polyaniline/Bentonite (Zn@PA/BE) as Multifunctional Photocatalyst under Visible Light. *Int. J. Environ. Anal. Chem.* **2022**. 1.
(36) Shaban, M.; Abukhadra, M. R.; Shahien, M. G.; Khan, A. A. P. Upgraded Modified Forms of Bituminous Coal for the Removal of Safranin-T Dye from Aqueous Solution. *Environmental Science and Pollution Research.* **2017**, *24*, 18135−18151.
(37) Li, L.; Zhang, Y.; Lu, H.; Wang, Y.; Xu, J.; Zhu, J.; Zhang, C.; Liu, T. Cryopolymerization Enables Anisotropic Polyaniline Hybrid

Hydrogels with Superelasticity and Highly Deformation-Tolerant Electrochemical Energy Storage. *Nat. Commun.* **2020**, *11*, 62 DOI: 10.1038/s41467-019-13959-9.
(38) Mooss, V. A.; Hamza, F.; Zinjarde, S. S.; Athawale, A. A. Polyurethane Films Modified with Polyaniline-Zinc Oxide Nanocomposites for Biofouling Mitigation. *Chem. Eng. J.* **2019**, *359*, 1400−1410.
(39) Vivas, E. L.; Cho, K. Efficient Adsorptive Removal of Cobalt(II) Ions from Water by Dicalcium Phosphate Dihydrate. *J. Environ. Manage.* **2021**, *283*, No. 111990.
(40) Bazan-Wozniak, A.; Nosal-Wiercińska, A.; Yilmaz, S.; Pietrzak, R. Low-Rank Coals as Precursors of Effective Carbonaceous Adsorbents for the Removal of Rhodamine B. *J. Mol. Liq.* **2023**, *389*, No. 122949.
(41) Mousavi, S. A.; Kamarehie, B.; Almasi, A.; Darvishmotevalli, M.; Salari, M.; Moradnia, M.; Azimi, F.; Ghaderpoori, M.; Neyazi, Z.; Karami, M. A. Removal of Rhodamine B from Aqueous Solution by Stalk Corn Activated Carbon: Adsorption and Kinetic Study. *Biomass Convers. Biorefinery* **2023**, *13* (9), 7927−7936.
(42) Du, P.; Zhang, J.; Cai, Z.; Ge, F. High Adsorption of Cationic Dyes from Aqueous Solution Using Worm-like Porous Nanosilica: Isotherm. *Kinetics and Thermodynamics. Mater. Today Commun.* **2023**, *35*, No. 105697.
(43) El Qada, E. Kinetic Behavior of the Adsorption of Malachite Green Using Jordanian Diatomite as Adsorbent. *Jordanian Journal of Engineering and Chemical Industries (Jjeci).* **2020**, *3*, 1−10.
(44) Salam, M. A.; Abukhadra, M. R.; Mostafa, M. Effective Decontamination of As(V), Hg(II), and U(VI) Toxic Ions from Water Using Novel Muscovite/Zeolite Aluminosilicate Composite: Adsorption Behavior and Mechanism. *Environ. Sci. Pollut. Res.* **2020**, *27* (12), 13247−13260.
(45) Lin, X.; Xie, Y.; Lu, H.; Xin, Y.; Altaf, R.; Zhu, S.; Liu, D. Facile Preparation of Dual La-Zr Modified Magnetite Adsorbents for Efficient and Selective Phosphorus Recovery. *Chem. Eng. J.* **2021**, *413*, No. 127530.
(46) Albukhari, S. M.; Salam, M. A.; Abukhadra, M. R. Effective Retention of Inorganic Selenium Ions (Se (VI) and Se (IV)) Using Novel Sodalite Structures from Muscovite; Characterization and Mechanism. *J. Taiwan Inst. Chem. Eng.* **2021**, *120*, 116−126.
(47) Jiang, Y.; Abukhadra, M. R.; Refay, N. M.; Sharaf, M. F.; El-Meligy, M. A.; Awwad, E. M. Synthesis of Chitosan/MCM-48 and β-Cyclodextrin/MCM-48 Composites as Bio-Adsorbents for Environmental Removal of Cd2+ Ions; Kinetic and Equilibrium Studies. *React. Funct. Polym.* **2020**, *154*, No. 104675.
(48) Sherlala, A. I. A.; Raman, A. A. A.; Bello, M. M.; Buthiyappan, A. Adsorption of Arsenic Using Chitosan Magnetic Graphene Oxide Nanocomposite. *J. Environ. Manage.* **2019**, *246*, 547−556.
(49) Huang, Y.; Zeng, X.; Guo, L.; Lan, J.; Zhang, L.; Cao, D. Heavy Metal Ion Removal of Wastewater by Zeolite-Imidazolate Frameworks. *Sep. Purif. Technol.* **2018**, *194*, 462−469.
(50) Jasper, E. E.; Ajibola, V. O.; Onwuka, J. C. Nonlinear Regression Analysis of the Sorption of Crystal Violet and Methylene Blue from Aqueous Solutions onto an Agro-Waste Derived Activated Carbon. *Appl. Water Sci.* **2020**, *10* (6), 132.
(51) Abukhadra, M. R.; Dardir, F. M.; Shaban, M.; Ahmed, E. A.; Soliman, M. F. Superior Removal of Co2+, Cu2+ and Zn2+ Contaminants from Water Utilizing Spongy Ni/Fe Carbonate−Fluorapatite; Preparation, Application and Mechanism. *Ecotoxicol. Environ. Saf.* **2018**, *157*, 358−368.
(52) Shaban, M.; Abukhadra, M. R.; Shahien, M. G.; Khan, A. A. P. Upgraded modified forms of bituminous coal for the removal of safranin-T dye from aqueous solution. *Environ. Sci. Pollut. Res.* **2017**, *24* (22), 18135−18151.
(53) Dawodu, F. A; Akpomie, G. K, and A. M. A. 2012IJSER2.Pdf. International Journal of Scientific and Engineering Research **2012**. https://www.researchgate.net/publication/301358615%0AEquilibrium.
(54) Mobarak, M.; Ali, R. A. M.; Seliem, M. K. Chitosan/Activated Coal Composite as an Effective Adsorbent for Mn(VII): Modeling and Interpretation of Physicochemical Parameters. *Int. J. Biol. Macromol.* **2021**, *186*, 750−758.
(55) Ashraf, M. T.; AlHammadi, A. A.; El-Sherbeeny, A. M.; Alhammadi, S.; Al Zoubi, W.; Ko, Y. G.; Abukhadra, M. R. Synthesis of Cellulose Fibers/Zeolite-A Nanocomposite as an Environmental Adsorbent for Organic and Inorganic Selenium Ions; Characterization and Advanced Equilibrium Studies. *J. Mol. Liq.* **2022**, *360*, No. 119573.
(56) Dhaouadi, F.; Sellaoui, L.; Reynel-Ávila, H. E.; Landín-Sandoval, V.; Mendoza-Castillo, D. I.; Jaime-Leal, J. E.; Lima, E. C.; Bonilla-Petriciolet, A.; Lamine, A. B. Adsorption Mechanism of Zn2+, Ni2+, Cd2+, and Cu2+ Ions by Carbon-Based Adsorbents: Interpretation of the Adsorption Isotherms via Physical Modelling. *Environ. Sci. Pollut. Res.* **2021**, *28*, 30943−30954.
(57) Abukhadra, M. R.; Saad, I.; Al Othman, S. I.; Alfassam, H. E.; Allam, A. A. Insight into the Synergetic, Steric and Energetic Properties of Zeolitization and Cellulose Fiber Functionalization of Diatomite during the Adsorption of Cd(II): Advanced Equilibrium Studies. *RSC Adv.* **2023**, *13* (34), 23601−23618.
(58) Dhaouadi, F.; Sellaoui, L.; Badawi, M.; Reynel-Ávila, H. E.; Mendoza-Castillo, D. I.; Jaime-Leal, J. E.; Bonilla-Petriciolet, A.; Lamine, A. B. Statistical Physics Interpretation of the Adsorption Mechanism of Pb2+, Cd2+ and Ni2+ on Chicken Feathers. *J. Mol. Liq.* **2020**, *319*, No. 114168.
(59) Sellaoui, L.; Ali, J.; Badawi, M.; Bonilla-Petriciolet, A.; Chen, Z. Understanding the Adsorption Mechanism of Ag+ and Hg2+ on Functionalized Layered Double Hydroxide via Statistical Physics Modeling. *Appl. Clay Sci.* **2020**, *198*, No. 105828.
(60) Ali, R. A. M.; Mobarak, M.; Badawy, A. M.; Lima, E. C.; Seliem, M. K.; Ramadan, H. S. New Insights into the Surface Oxidation Role in Enhancing Congo Red Dye Uptake by Egyptian Ilmenite Ore: Experiments and Physicochemical Interpretations. *Surfaces and Interfaces* **2021**, *26*, No. 101316.
(61) Sellaoui, L.; Guedidi, H.; SarraWjihi, S.; Reinert, L.; Knani, S.; Duclaux, L.; Ben Lamine, A. Experimental and Theoretical Studies of Adsorption of Ibuprofen on Raw and Two Chemically Modified Activated Carbons: New Physicochemical Interpretations. *RSC Adv.* **2016**, *6* (15), 12363−12373.

https://doi.org/10.1021/acsomega.3c07355
ACS Omega 2023, 8, 47210−47223